

Technoeconomic Analysis of Alternative Solarized s-CO₂ Brayton Cycle Configurations

Clifford K. Ho

Sandia National Laboratories,
Albuquerque 87185-1127, NM
e-mail: ckh@sandia.gov

Matthew Carlson

Sandia National Laboratories,
Albuquerque 87185-1127, NM

Pardeep Garg

Indian Institute of Science,
Bangalore 560012, India

Pramod Kumar

Indian Institute of Science,
Bangalore 560012, India

This paper evaluates cost and performance tradeoffs of alternative supercritical carbon dioxide (s-CO₂) closed-loop Brayton cycle configurations with a concentrated solar heat source. Alternative s-CO₂ power cycle configurations include simple, recompression, cascaded, and partial cooling cycles. Results show that the simple closed-loop Brayton cycle yielded the lowest power-block component costs while allowing variable temperature differentials across the s-CO₂ heating source, depending on the level of recuperation. Lower temperature differentials led to higher sensible storage costs, but cycle configurations with lower temperature differentials (higher recuperation) yielded higher cycle efficiencies and lower solar collector and receiver costs. The cycles with higher efficiencies (simple recuperated, recompression, and partial cooling) yielded the lowest overall solar and power-block component costs for a prescribed power output.

[DOI: 10.1115/1.4033573]

1 Introduction

Previous research has investigated the feasibility and performance of integrating concentrating solar technologies with s-CO₂ closed-loop Brayton power cycles [1–4]. Figure 1 shows a schematic of a solar-driven, indirectly heated, closed-loop s-CO₂ Brayton power cycle. Past studies have shown that simple recompression s-CO₂ cycles can theoretically reach 50% thermal-to-electric efficiency with a turbine inlet temperature > 700 °C and pressure > 20 MPa [3–5]. The use of recompression with significant recuperation increases the cycle efficiency and reduces the required heat addition from the solar receiver or heat exchanger; a temperature difference of only ~100–150 °C is required across the receiver or heat exchanger. However, this relatively small temperature difference can increase the required mass flow rate and inventory of sensible heat-transfer media being used in the concentrating solar power subsystem (e.g., molten salt, solid particles) for a prescribed power generation capacity, which increases associated costs. Other s-CO₂ Brayton cycle configurations without recompression or with reduced recuperation can increase the temperature difference across the heat exchanger and reduce the costs of the heat-transfer/storage media as well as component costs of the power block. These benefits come at the expense of a lower thermal-to-electric efficiency, requiring greater thermal energy input and greater costs associated with the solar collector field (heliostats) and solar receiver. This paper evaluates these performance and cost tradeoffs for several alternative s-CO₂ closed-loop Brayton configurations with a concentrating solar heat source.

2 Alternative s-CO₂ Cycle Configurations

2.1 Simple Closed Brayton Cycle (SCBC). The SCBC, also called the recuperated closed Brayton cycle, is the simplest s-CO₂ power conversion cycle configuration, consisting of a single stage

each of compression, recuperation, and expansion as shown in (Fig. 2). This power cycle pattern has been used for a number of working fluids and applications including air for stationary power generation [6], helium for advanced nuclear reactor concepts [7], a variety of noble gas and other mixtures for space power applications, and recently with supercritical fluids.

Implementations with ideal gas working fluids almost always use intercooling, recuperation, or both to improve cycle efficiency at moderate increments of cost. Intercooling reduces the compression work within a cycle and directly increases the work output side of the efficiency equation. Recuperation reduces the heating required for the same cycle power level which directly reduces the heat input side of the efficiency equation.

For cycles operating with real gases near their critical point, the advantage of intercooling is significantly reduced as the back-work ratio is already very low. s-CO₂ CBCs can achieve high efficiencies but are limited by a pinch-point that occurs in the recuperation process [8].

The SCBC is the first to be commercialized by Echogen Power Systems, Inc. for waste heat recovery applications [9–11], although it should be noted that their EPS100 layout has a motor-driven pump/compressor and a turbine generator rather than a single-shaft system as depicted in the figure [12]. Analysis in Ref. [11] suggests that a SCBC could provide 10–20% lower leveled cost as compared with steam Rankine waste heat recovery systems, primarily due to lower component size and costs and reduced system footprint.

2.2 Recompression Closed Brayton Cycle (RCBC). The RCBC is a modification of the SCBC which uses two-stages of recuperation and partial recompression in order to improve cycle efficiency as shown in Fig. 3. This arrangement, first suggested by Angelino [13], avoids the effect of the pinch point encountered in SCBCs as additional recuperation is provided. More detailed discussions of pinch point limitation in SCBCs and RCBCs can be found in several previous works [8,14,15].

After early work by Feher and Hoffmann [8,16] and Angelino [13,17–21], this cycle gained renewed interest in 2004 based on an analysis of RCBCs for nuclear power applications [22]. Theoretical efficiencies were found to be between 45% and 50% above 550 °C, providing significant benefit over alternative steam cycles. The primary heat exchanger temperature rise of 150 °C was also well-matched to reactor core temperature gradients.

Contributed by the Solar Energy Division of ASME for publication in the JOURNAL OF SOLAR ENERGY ENGINEERING: INCLUDING WIND ENERGY AND BUILDING ENERGY CONSERVATION. Manuscript received September 18, 2015; final manuscript received March 22, 2016; published online July 12, 2016. Assoc. Editor: Carlos F. M. Coimbra.

The United States Government retains, and by accepting the article for publication, the publisher acknowledges that the United States Government retains, a nonexclusive, paid-up, irrevocable, worldwide license to publish or reproduce the published form of this work, or allow others to do so, for United States government purposes.

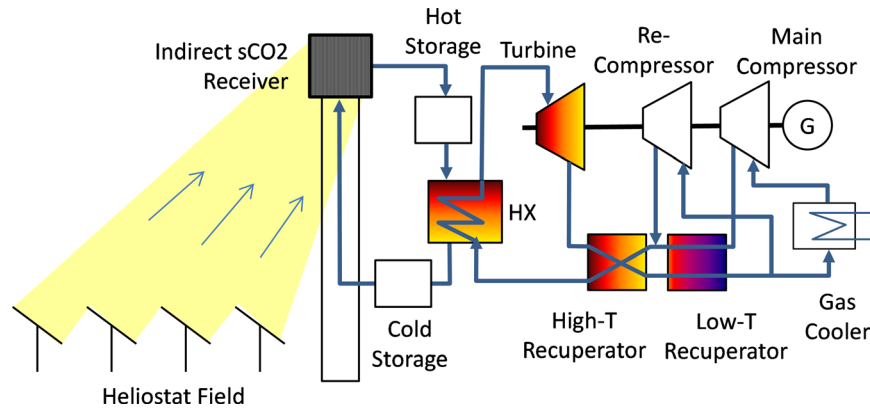


Fig. 1 Schematic of a solar-driven, indirectly heated, closed-loop supercritical CO₂ Brayton power cycle

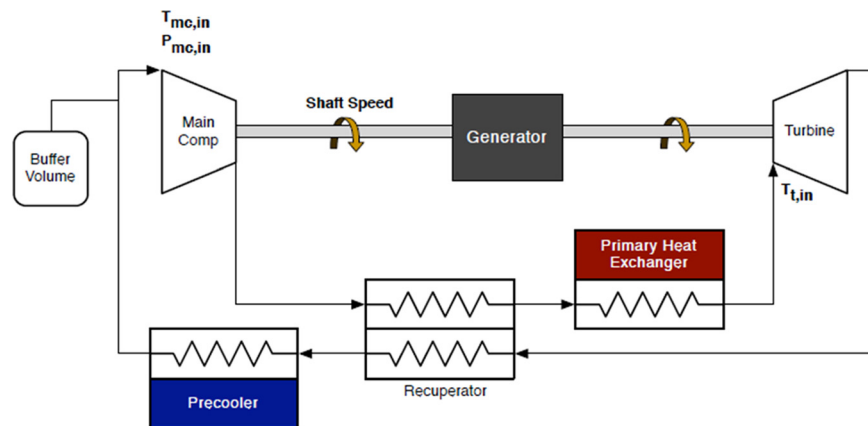


Fig. 2 A flow diagram of a SCBC configuration

The studies by Dostal et al. [22] and Dyreby et al. [14] are notable for their work optimizing RCBCs for nuclear and concentrating solar applications.

2.3 Cascaded Closed Brayton Cycle (CCBC). CCBCs are a variation aimed at maximizing utilization of a fluid stream rather than the thermal efficiency of the cycle. These cycles have several turbines provided with a cascade of several inlet temperatures using several steps of recuperation as shown in Fig. 4. This approach allows for higher specific power while also varying recuperator flow rates sufficiently to avoid the impact of pinch conditions.

Kimzey performed an analysis of three CCBC configurations optimized for a Siemens H Class and a GE LM6000 combined cycle gas turbine systems [23]. Cycle efficiencies ranged from 25 to 35%, however, the net power output of the CCBC for the large H Class system was below that of the current steam bottoming cycles and only slightly above steam for the LM6000. Despite negligible performance improvement, s-CO₂-based cascaded cycles may still reduce overall combined cycle cost due to their reduced equipment volume and footprint as suggested by work at Echogen.

2.4 Combination Bifurcation With Intercooler (CBI or Partial Cooling). High turbine inlet pressures (~300 bar or 30 MPa) lower the temperature rating of the material used in the power block and increase the need for expensive high-temperature materials. Redesigning the thermodynamic cycle in such a way that the optimum efficiencies of ~45% are obtained at ~150 bar (15 MPa) turbine inlet pressure can bring down the cost associated

with the power block. In this regard, a new cycle known as CBI cycle was analyzed and found to offer efficiencies as high as the s-CO₂ cycle but at lower high side pressures [24]. Since this cycle involves condensation during the heat rejection process, CO₂ is not a suitable candidate for this cycle owing to its low critical temperature (~31 °C). One possible alternate is to blend CO₂ with a thermodynamically similar fluid to raise its critical temperature. 48.5% of propane in the balance of CO₂ has a critical temperature of ~63 °C making the condensation during heat rejection viable even at warmer temperatures. However, issues related to the thermal stability of the proposed mixture at high temperatures need to be addressed adequately. Since its thermodynamic performance is found to be marginally superior to that of the pure CO₂, this mixture serves as a potential alternative power cycle fluid in the CBI cycle discussed below (Figs. 3 and 4).

Figure 5 shows a schematic of the CBI cycle. Major components in the power block are the pump, compressor, regenerator, heater, turbine, gas cooler, and condenser. Thermodynamic state 1 in the cycle is the saturated liquid corresponding to minimum cycle temperature from where it is pumped to state 2. Process 2–3 represents the heat addition, a part of which is supplied internally by two regenerators from states 2 to 8 and 8 to 5, and the rest is provided externally by a heater from 5 to 3. Turbine exhaust acts as the hot side of these regenerators. In Regenerator₁, turbine exhaust cools down from 4 to 6, heating the high pressure working fluid from 8 to 5. Further cooling on the low pressure side from 6 to 9 is achieved by transferring heat to the pump outlet in which it is heated from 2 to 8. To minimize the work of compression, the low pressure side is cooled to a minimum cycle temperature (state 10) which is followed by compression of the working fluid to the

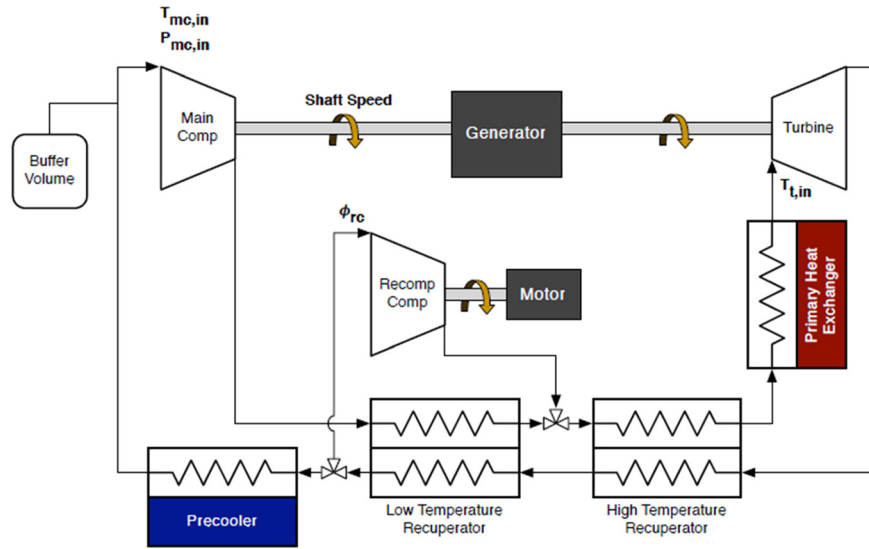


Fig. 3 A flow diagram of a supercritical CO₂ RCBC

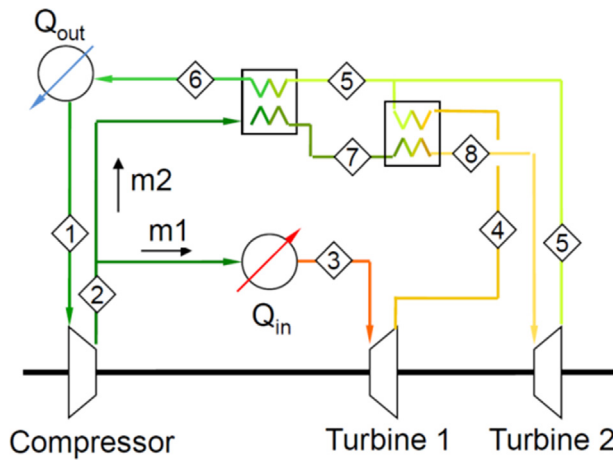


Fig. 4 A flow diagram of the first CCBC analyzed by Kimzey [23]

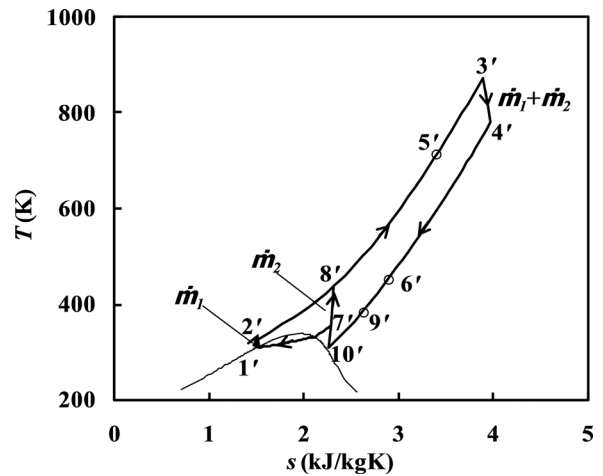


Fig. 6 T - s diagram of CBI cycle [24]

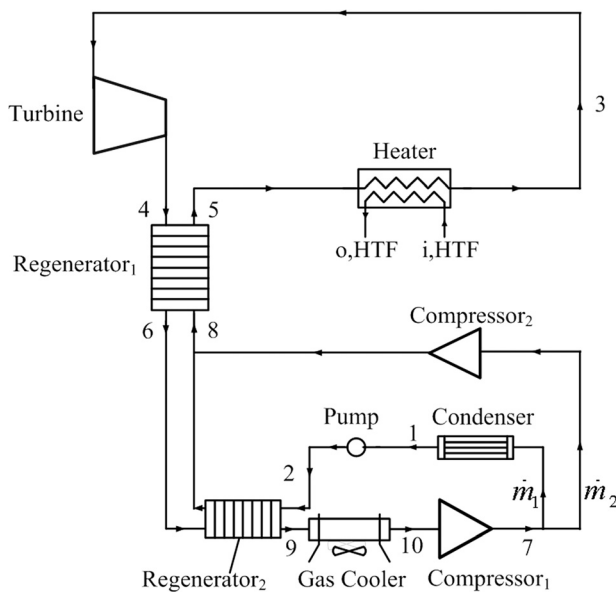


Fig. 5 Schematic of a CBI cycle [24]

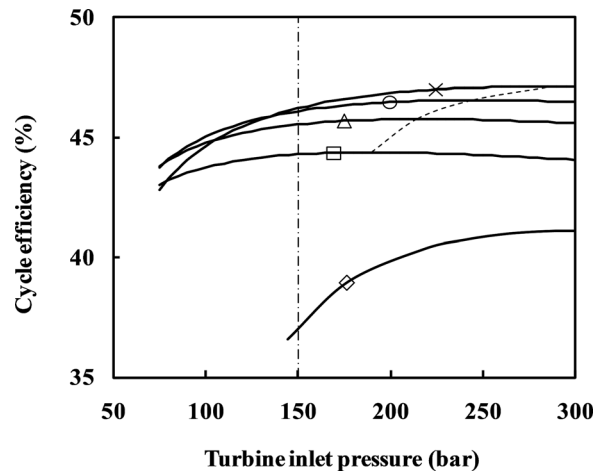


Fig. 7 CBI cycle efficiency versus turbine inlet pressure for various turbine outlet pressures. Legend: \square $p_4 = 10$ bar, Δ $p_4 = 15$ bar, \circ $p_4 = 20$ bar, \times $p_4 = 26$ bar, \diamond $p_4 = 75$ bar. (1 bar = 100 kPa).

pump inlet pressure. At this point, the working fluid is bifurcated into two streams: one that is directly compressed from 7 to 8 and the other that is first condensed to give saturated liquid (state 1) and then pumped to 2. Further, the two streams unite again at state 8. The cycle is represented on a T - s diagram in Fig. 6.

The key significance of the CBI cycle is its higher efficiency at lower operating pressures as observed in Fig. 7. Here, turbine inlet and outlet pressure (p_3 and p_4 , respectively) are the independent parameters. While the lower limit of p_4 is set to 10 bar (1 MPa) to avoid a drop in cycle efficiency, the upper limit is 26 bar (2.6 MPa) to keep the state 10 in a dry zone. Optimum cycle efficiency as well as corresponding optimum p_3 increases with an increase in p_4 with a maximum efficiency of $\sim 47\%$ at $p_4 = 26$ bar (2.6 MPa) and $p_3 = 250$ bar (25 MPa). However, there are diminishing returns on efficiency beyond $p_3 = 150$ bar (15 MPa) where the maximum efficiency observed for the CBI cycle is 46.2%. For the sake of comparison, the CBI cycle is compared with the supercritical CO_2 cycle under identical operating conditions. The curve corresponding to the turbine outlet pressure of 75 bar in Fig. 7 represents the case of an s- CO_2 cycle. It can be observed that the best efficiency of the CBI cycle is about 6% higher than that of the s- CO_2 cycle. This is attributed to the lower irreversibility generation in the two-stage regeneration effect of the former compared to the single-stage regeneration in the latter. Further, in the case of the CBI cycle, there is an added advantage of lower efficiency amplitude with respect to turbine inlet pressure making it a promising cycle even at low pressures.

It should be noted that the partial cooling s- CO_2 cycle described in Refs. [3] and [4] is similar to the CBI cycle if the working fluid is 100% s- CO_2 , although the CBI cycle is also multiphase due to the presence of the condenser and low-pressure pump leg from states 7 to 2.

3 Cost and Performance of Alternative s- CO_2 Cycle Configurations

System performance and cost must be optimized together for a given application. Previous studies by Driscoll and Hejzlar [25] and Dostal et al. [22] relay primarily on \$/kg costing data quoted informally from Heatric and turbomachinery studies done by Schlenker [26] in the 1970s for very large helium Brayton cycle nuclear power conversion.

More recent data for commercial equipment with applicability to s- CO_2 power cycles are available from the Engineering Sciences Data Unit [27] and Peters et al. [28] for heat exchanger and turbomachinery costs, respectively. An example set of power-law scaling relationships from these sources is provided in Table 1 for reference, though the costs presented in this paper are interpolated from the complete data set rather than using the fitting equations.

The ESDU heat exchanger cost data scales with unit type, hot and cold-side fluids, and unit performance as described by the overall conductance area product (UA) value in (W/K). For the cycles analyzed in this paper, the primary heat exchanger is

Table 1 Example equipment cost scaling from Refs. [26] and [27]

	Approximate cost scaling
Primary heat exchanger (\$)	$17.5(\text{UA}(\text{W/K}))^{0.8778}$
Recuperator (\$)	$5.2(\text{UA}(\text{W/K}))^{0.8933}$
Air coolers/condensers (\$) ^a	$76.25(\text{UA}(\text{W/K}))^{0.8919}$
Compressors (\$) ^b	$643.15(\dot{W}(\text{kW}))^{0.9142}$
Turbines (\$) ^c	$9923.7(\dot{W}(\text{kW}))^{0.5886}$

^aIncludes factor of 2.5 for stainless steel materials.

^bIncludes factors of 2.5 and 0.2 for stainless steel construction and density ratio of air and CO_2 at 8 MPa.

^cInclude factor of 3 for nickel alloy construction.

assumed to be a printed-circuit heat exchanger (PCHE) with high-pressure gas on the cold side and high-viscosity (20 cP) fluid on the hot side in order to represent the flow of particles from a thermal storage reservoir. It should be noted that this arrangement is used only to estimate the cost of a particle to s- CO_2 diffusion-bonded heat exchanger which would have microchannels on the s- CO_2 side and large passages on the particle side similar to that required for a high-viscosity liquid either formed as part of the PCHE core or created by arranging PCHE plates within the particle flow. Recuperators are also assumed to be PCHE-style units with high-pressure gas on both sides. Finally, all cooling is assumed to be accomplished with A-frame, finned-tube air coolers. The air cooler data are modified by a factor of 2.5 to account for the use of stainless rather than carbon steel as directed in the original source, which is consistent with the assumed use of stainless steel for both the recuperators and particle/s- CO_2 heat exchanger.

Peters et al. [28] provide a number of cost scaling curves for a variety of industrial equipment including axial and radial turbines and motor and turbine-driven compressors. These curves deviate from power-law relationships at lower capacities, but are well-fit by the equations in Table 1 for the range of interest. Both relations are based on the power required by or delivered to the equipment handling air and other industrial gases, and are modified by factors of 2.5 for compressors constructed of stainless steel and 3 for turbines constructed of nickel alloys rather than carbon steel. It is assumed that conventional nickel alloys such as 625 and 718 are used rather than 740 which would have a significantly larger and more uncertain cost factor. The compressor data is further modified by a density ratio factor of 0.2 to account for the increased power density of CO_2 necessary when assuming identical volumetric flow rate and head rise of the CO_2 compressor to the air compressor. This value is adjusted from 0.2 up to 0.8 with decreasing density as the compressor inlet pressure is lowered for the same compressor inlet temperature when evaluating the SCBC cycle.

Design parameters were chosen from literature for the RCBC, CCBC, and CBI cycles described previously as summarized in Table 2. All cycles operate at or above a 600 °C turbine inlet temperature and are designed for electrical power outputs of at least 100 MWe, with most originally having a turbine inlet pressure near 30 MPa that was adjusted down to 20 MPa due to expected material limitations on pressure containment discussed later.

Table 2 Power cycle design, performance, and cost

	SCBC [14]	RCBC [14]	CCBC [23]	CBI [24]	
Net power (MWe)	100	100	100	133	100
Efficiency (%)	16	46	46	28	51
T_{max} (°C)	700	700	700	600	700
T_{max} (MPa)	20	20	20	27.6	15
P_{min} (MPa)	6.4	8.0	7.3	8.5	2.6
P_{int} (MPa)	N/A	N/A	N/A	N/A	5.0
$T_{\text{comp,min}}$ (°C)	55	55	55	37	35
η_{comp} (%)	90	90	90	85	90
η_{exp} (%)	90	90	90	90	90
f_{rec} or f_{cascaded} (%)	N/A	N/A	11.5	47.5	40
$\Delta T_{\text{HTF,min}}$ (°C)	25	25	25	25	25
$T_{\text{air,min}}$ (°C)	30	30	30	30	30
ΔT_{HTR} (°C)	540	172	170	518	159
\dot{C}_{HTF} (MW/K)	1.39	1.53	1.27	0.919	1.21
\dot{q}_{HTF} (MWth)	623	220	216	449	192
Heater (\$/kWe)	381	212	322	281	292
Recuperation (\$/kWe)	0.00	243	244	122	259
Cooling (\$/kWe)	545	85	154	574	350
Compression (\$/kWe)	423	230	147	80	74
Expansion (\$/kWe)	136	128	135	138	120
Total (\$/kWe)	1485	898	1002	914	1095

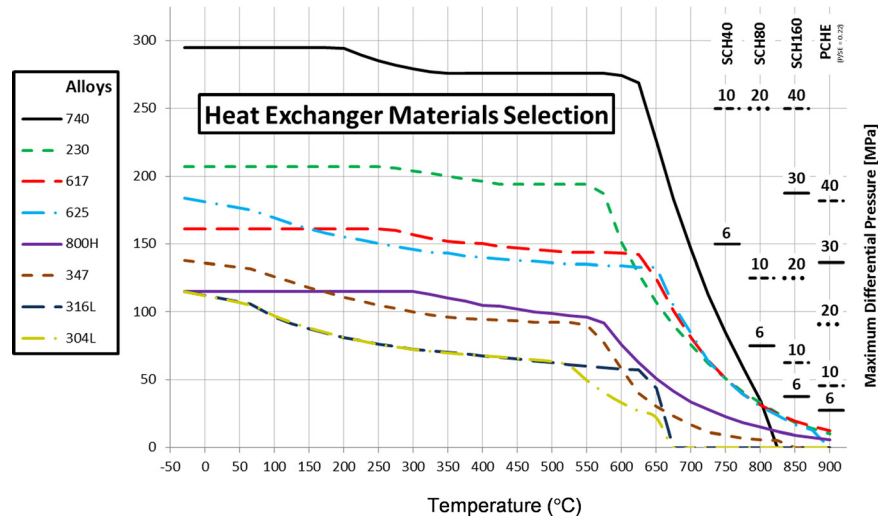


Fig. 8 Heat exchanger material selection curves from the ASME Boiler and Pressure Vessel code

The boundary conditions for each cycle configuration are chosen to provide a fair comparison for the same application. SunShot goals, initiated as part of the U.S. Department of Energy’s Solar Energy Technologies program, suggest a low-temperature limitation of 55°C based on an ambient temperature of 40°C for dry-cooled cycles. However, the CCBC and CBI cycles have not been optimized for dry cooling and would not be possible to analyze at 40°C. Therefore, all cycles are analyzed at an ambient temperature of 30°C. This introduces an additional cost increment for cooling equipment because the CCBC and CBI cycles have very low approach temperatures as compared with the other cycles.

Re-optimization of the CCBC cycle is outside the scope of this paper but is expected to involve reduction of the high-side pressure and an increase of the low-side pressure, which at higher turbine inlet temperatures will lower both efficiency and cost. Re-optimization of the CBI cycle is more difficult as the mixture fractions of CO₂ and propane must be changed to retain the benefits of the partial cooling architecture. Due to unique CBI cycle constraints to mitigate flammability, it is difficult to speculate on the impact of a dry-cooled design point.

The turbine inlet temperature will not likely be an issue as uncooled low-pressure gas turbine blades operate at temperatures of 1150°C. Therefore, the high-temperature points in each cycle would likely be governed by pressure containment requirements based on the combination of temperature, pressure, and material used in the particle/s-CO₂ heat exchanger.

Figure 8 provides ASME Boiler and Pressure Vessel code allowable strengths versus temperature for several candidate s-CO₂ materials, as well as reference lines for maximum allowable differential pressures assuming different part thicknesses including schedule 40, 80, and 160 piping and typical PCHEs. Note that these reference lines represent typical wall thickness, while larger thicknesses are possible for both piping and heat exchangers.

The curves in Fig. 8 can be grouped into roughly three categories based on their maximum service temperature at differential pressures of 20 MPa: stainless steel 347 and alloy 800 H at 600°C, Alloys 617 and 625 at 700°C, and Inconel 740 and 750°C. Note that dual-certified 316/316L can be used up to 625°C using much larger vessel wall thicknesses. There is limited commercial experience with Inconel 740 in Advanced Ultra-Supercritical coal plants operating in this range of material strength, leaving Alloys 617 and 625 as the most reasonable constraint on cycle operating conditions.

The RCBC design point is based on an optimization study by Dyreby et al. [14] assuming a normalized recuperator conductance of 0.2 (MW/K MWe).

The SCBC data are optimized using the cost models to inform the design, resulting in different balancing points between high back-work ratios and compression costs at low compressor inlet pressures and high cooling costs at high compressor inlet pressures. A pressure of 6.4 MPa is chosen for the unrecuperated cycle while a pressure of 8 MPa is used for the recuperated cycle.

The general trend in cycle cost is as expected, with more complex cycles such as the RCBC and CBI cycle realizing higher efficiency at a penalty of higher equipment cost. However, the spread in cycle costs ranges from \$830/kWe for the recuperated SCBC to \$1580/kWe for the CCBC. The recuperated SCBC demonstrates a very low cost considering its high efficiency of 46%, compared to RCBC and CBI cycle efficiencies. While higher theoretical efficiencies have been calculated by others, as discussed by Dyreby et al. [14] and Neises and Turchi [4], most of these analysis assumed impractically large recuperators by specifying heat exchanger performance using an effectiveness or approach temperature value rather than a UA value, and by assuming turbine inlet pressures higher than can be practically achieved using conventional materials.

The SCBC and RCBC cycles have identical efficiencies and similar performance due to the elevated compressor inlet temperature of 55°C. This higher compressor inlet temperature moves the recuperation process away from the critical point of CO₂, reducing the effect of pinching caused by property variations near the critical point and in turn the benefit of the more complex RCBC layout. This has been observed and discussed previously by Dyreby et al. [14].

Comparing the two SCBC layouts, adding recuperation has a significant effect on equipment cost due to the increased compression and cooling requirements.

The RCBC, recuperated SCBC, and CBI cycles that optimize efficiency have similar required heat source capacitance rates around 1.3 MW/K and 160–170°C temperature differentials. The unrecuperated SCBC and CCBC cycles both provide temperature differentials higher than 500°C with similar capacitance rates, but at significant efficiency penalties of 20–35% points and large increases in cost.

Although mentioned previously, it should be noted again that the CCBC and CBI cycles are impacted by significant cooling costs because they were originally optimized for wet cooling rather than dry cooling temperatures. For this analysis they were

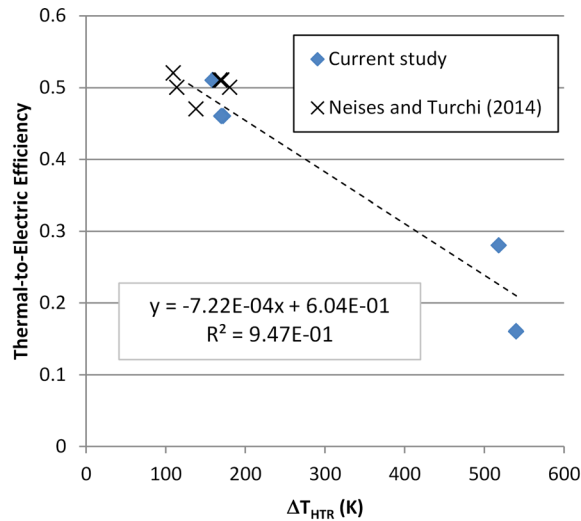


Fig. 9 Thermal-to-electric efficiency of various s-CO₂ closed Brayton cycle configurations as a function of temperature difference across the primary heat source to the power block (ΔT_{HTR})

not re-optimized, and so the lower compressor inlet temperature combined with high ambient temperatures produce a close approach temperature in the cooler, scaling both the size and cost.

Based on these results, the recuperated SCBC appears to be a good candidate for a concentrating solar power plant with sensible storage media. This cycle provides the lowest cost of the various configurations, while still providing high efficiency and a large primary heat-exchanger temperature differential.

4 Cost and Performance Impacts on Concentrating Solar Components

As described in Ref. [4], the performance characteristics of alternative s-CO₂ cycle configurations can impact the cost and performance of concentrating solar power subsystems and components. Configurations that require small temperature differences across the primary heat exchanger can require larger mass flow rates of the heat-transfer/storage media. This can increase the required inventory and cost of the storage media and containment for a desired storage capacity. The relationship between the storage media mass flow rate, \dot{m} , temperature difference across the primary heat exchanger, ΔT_{HTR} (K), and power required, \dot{Q} (W), is derived from an energy balance on the storage media passing through the heat exchanger with the s-CO₂ working fluid

$$\dot{Q} = \dot{m} c_p \Delta T_{HTR} \quad (1)$$

where c_p is the specific heat of the storage media (J/kg K). The required power, \dot{Q} (W), depends on the thermal-to-electric efficiency of the different s-CO₂ cycle configurations (see Table 2). The required thermal input to the s-CO₂ cycle also impacts the requirements and costs of the solar collector field and receiver.

Based on the data in Table 2 and from Ref. [4], Fig. 9 plots the thermal-to-electric efficiency of alternative s-CO₂ cycles as a function of the temperature difference across the primary s-CO₂ heater. A linear curve fit matches the available data well, showing an inverse correlation between the efficiency and temperature difference. Smaller temperature differences across the primary s-CO₂ heater result from greater recuperation within the cycle configuration. It should be noted that the primary s-CO₂ heater could be either the solar receiver (for direct s-CO₂ heating) or the heat exchanger between the thermal storage media and the s-CO₂ (for indirect heating of s-CO₂). Ho et al. [1] provides an overview of direct and indirect s-CO₂ solar heating configurations.

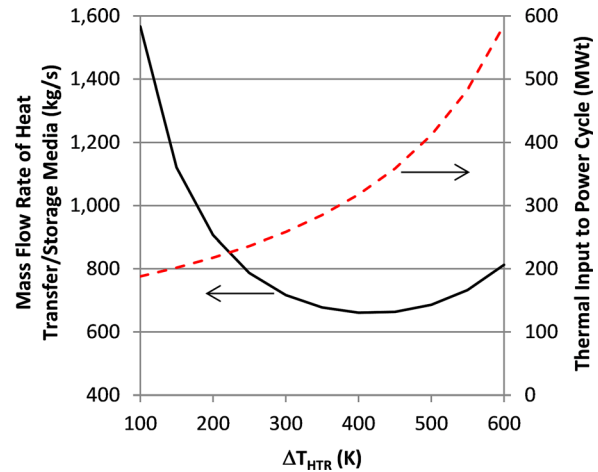


Fig. 10 Mass flow rate of heat-transfer/storage media and required thermal input as a function of temperature difference across the heat source to the power block (ΔT_{HTR})

The inverse correlation between thermal-to-electric efficiency and temperature difference is used to plot the required mass flow rate of the heat-transfer/storage media (Eq. (1)) and thermal input to the power cycle as a function of the temperature difference across the primary s-CO₂ heater (Fig. 10). As the temperature difference increases, the thermal efficiency decreases, resulting in a greater required thermal input to the power cycle. Equation (1) is then used to determine the heat-transfer/storage media mass flow rate as a function of temperature difference assuming a specific heat of 1200 J/kg K (for ceramic particles [29]); specific heat of HITEC molten salt is ~ 1300 J/kg K. There exists a tradeoff at higher temperature differences, which reduce the required mass flow rate for a given power input (Eq. (1)), and lower efficiencies at higher temperature differences (Fig. 9), which increases the required power input and mass flow rate. Figure 10 shows that the mass flow rate exhibits a minimum at a temperature difference of ~ 400 K assuming the efficiency correlation shown in Fig. 9. As the temperature difference increases beyond 400 K, the reduction in efficiency requires a greater thermal power input and, subsequently, mass flow rate that outweighs the reduction in required mass flow rate with increasing temperature difference.

These relations are used to determine the relative cost impacts on the solar heliostat field, receiver, and thermal storage system using design parameters shown in Table 3.

Figure 11 plots the heliostat cost as a function of power-cycle efficiency. Higher efficiencies reduce the required thermal input and, hence, the number of heliostats required to produce the prescribed power output. Results are shown for two different heliostat price points: a “current” heliostat cost of $\$200/\text{m}^2$ [30] and the DOE SunShot goal of $\$75/\text{m}^2$.

Figure 12 plots the solar receiver cost as a function of cycle efficiency. The costs are based on a current receiver cost of

Table 3 Design parameters used to estimate solar component costs

Turbine capacity (MWe)	100
Solar-field collection efficiency	0.6
Solar receiver efficiency	0.85
Solar multiple	2
Capacity factor	0.4
Specific heat of heat-transfer/storage media (J/kg K)	1200
Hours of storage	6
Average DNI ^a (W/m ²)	818

^aBased on hours of direct normal irradiance (DNI) > 500 W/m² per TMY3 data for Albuquerque, NM.

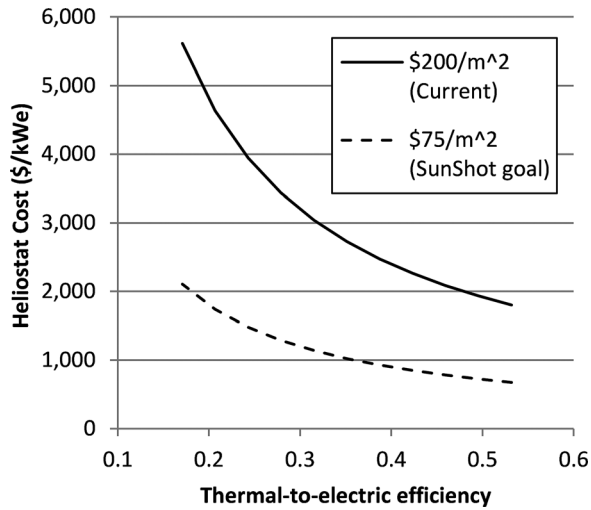


Fig. 11 HelioStat cost as a function of thermal-to-electric efficiency

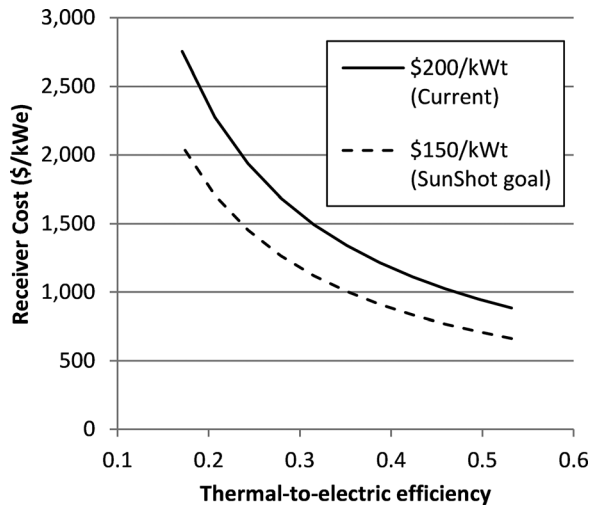


Fig. 12 Receiver cost as a function of thermal-to-electric efficiency

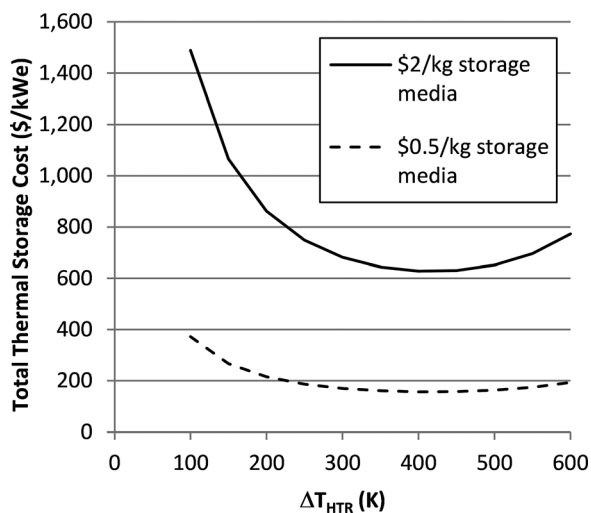


Fig. 13 Thermal storage cost as a function of temperature difference across the heat source to the power block (ΔT_{HTR})

Table 4 Solar component costs for alternative s-CO₂ cycle configurations

	SCBC	Recuperated SCBC	RCBC	CCBC	CBI
HelioStats (\$/kWe)	4120	1430	1430	2350	1290
Receiver (\$/kWe)	2570	895	895	1470	807
Storage (\$/kWe)	517	508	598	341	634
Total (\$/kWe)	7210	2840	2930	4170	2730

\$200/kWt [30] and a SunShot goal of \$150/kWt. Higher cycle efficiencies reduce the required thermal input, which reduces the associated size and costs of the solar receiver subsystem.

Figure 13 plots the thermal storage costs as a function of the temperature difference across the primary s-CO₂ heater. The mass flow rate of the heat-transfer/storage media shown in Fig. 10 was used to determine the required mass of storage media for 6 hrs of storage (including 10% additional mass for ullage space [31]). Kolb et al. show that the storage media cost comprises about half of the total storage system costs. Therefore, the total thermal storage cost shown in Fig. 13 was calculated as twice the storage media costs. Two storage media price points were assumed: \$0.5/kg and \$2/kg. Costs of sodium- and potassium-nitrate salts range between \$0.7/kg and \$1.5/kg (quote from SQM), and costs of bulk ceramic particles range between \$1.0/kg and \$1.3/kg (quote from CARBO). The trends in storage system cost follow the required mass flow rates as a function of temperature difference across the s-CO₂ heater as shown in Fig. 10.

Based on the relations discussed above, the costs of each concentrating solar component for the different cycle configurations can be determined. Table 4 summarizes the costs of the solar components for each of the alternative power cycle configurations considered in Secs. 2 and 3. The costs are calculated using the average of the two price points for the heliostats, receiver, and storage media shown in Figs. 11–13. Results show that the recuperated SCBC, RCBC, and CBI cycles yield the lowest overall solar costs. High cycle efficiencies of these configurations reduce the cost of the heliostats and the receiver (albeit at a slight expense of smaller temperature differences across the heater, which increases the cost of the storage system).

Table 5 summarizes the total solar and power-block costs for the different alternative power-cycle configurations considered. The recuperated SCBC, RCBC, and CBI cycles yield the lowest overall costs as a result of higher cycle efficiencies, which reduce the required thermal input to the power cycle and the associated costs of the heliostat field and solar receiver. This outweighed the increased costs associated with larger amounts of heat-transfer and storage materials required with lower temperature differences across the heat exchanger at the higher efficiencies.

5 Conclusions

Alternative s-CO₂ closed-loop Brayton cycles were evaluated in this paper to determine relative performance and cost impacts on both the power-block and concentrated solar heating components. Simple (SCBC), recompression (RCBC), cascaded (CCBC), and CBI (partial cooling) closed-loop Brayton cycles were evaluated. Results show that the recuperated SCBC, RCBC, and CBI cycles yield the lowest overall costs as a result of higher cycle efficiencies, which reduce the required thermal input to the power cycle and the associated costs of the heliostat field and solar receiver. Lower temperature differences across the primary s-CO₂ heater increase the required mass flow rate of the sensible heat-transfer/storage media, but the resulting cost increase is relatively small compared to the costs of the heliostats and solar receiver.

Additional factors not considered in this paper that will impact performance and cost include the following:

Table 5 Total costs for alternative s-CO₂ cycle configurations

	SCBC	Recuperated SCBC	RCBC	CCBC	CBI
Concentrating solar costs (\$/kWe)	7210	2840	2930	4170	2730
Power block costs (\$/kWe)	1485	898	1002	914	1095
Total costs (\$/kWe)	8690	3730	3930	5080	3830

- Need for materials that can withstand high temperatures (>700 °C) and/or pressures (>20 MPa) in the solar receiver, heat exchangers, storage, and turbomachinery.
- Configurations operating at high temperatures and low ΔT across the primary s-CO₂ heat exchanger will incur greater heat losses from the solar receiver than from a system with lower operating temperatures and larger ΔT. Greater heat losses will reduce the solar receiver efficiency and increase costs.
- Performance and cost parameters of a solar-driven s-CO₂ closed-loop Brayton cycle are still highly uncertain. Future studies should consider probabilistic analyses to quantify inherent uncertainties in cost and performance.
- Latent storage materials that have a phase-change temperature consistent with the turbine inlet temperature may be a good fit for the small temperature differentials required by recuperated cycles, potentially yielding better exergetic efficiencies.
- The thermodynamic and kinetic equilibrium of the mixed-gas CBI cycle especially at high temperatures will impact the thermodynamic performance and optimal operating conditions of the CBI cycle. Additional studies in this area are needed.

Acknowledgment

This research is based upon work supported in part by the Solar Energy Research Institute for India and the U.S. (SERIUS) funded jointly by the U.S. Department of Energy Subcontract No. DE AC36-08G028308 (Office of Science, Office of Basic Energy Sciences, and Energy Efficiency and Renewable Energy, Solar Energy Technology Program, with support from the Office of International Affairs) and the Government of India subcontract IUSSTF/JCERDC-SERIUS/2012 dated Nov. 22, 2012.

Sandia National Laboratories is a multiprogram laboratory managed and operated by Sandia Corporation, a wholly-owned subsidiary of Lockheed Martin Corporation, for the U.S. Department of Energy’s National Nuclear Security Administration under Contract No. DE-AC04-94AL85000. The U.S. Government retains and the publisher, by accepting the article for publication, acknowledges that the U.S. Government retains a nonexclusive, paid-up, irrevocable, world-wide license to publish or reproduce the published form of this manuscript, or allow others to do so, for U.S. Government purposes.

Nomenclature

- A = heat exchanger surface area (m²)
- c_p = specific heat of storage media (J/kg K)
- Ċ_{HTF} = capacitance rate of the heat-transfer fluid (W/K)
- CBI = combination bifurcation with intercooler
- CCBC = cascaded closed Brayton cycle
- f_{cascaded} = cascaded fraction of the total system mass flow rate
- f_{rec} = recompression fraction of the total system mass flow rate
- ṁ = mass flow rate (kg/s)
- P_{max} = maximum cycle pressure (Pa)
- P_{min} = minimum cycle pressure (Pa)
- PCHE = printed circuit heat exchanger
- Q̇ = required thermal power for cycle (W)

- q̇_{HTF} = heat-transfer rate from the heat-transfer fluid to the s-CO₂ (W)
- RCBC = recompression closed Brayton cycle
- SCBC = simple closed Brayton cycle
- s-CO₂ = supercritical carbon dioxide
- T_{comp,min} = temperature entering compressor (°C)
- T_{max} = maximum turbine inlet temperature (°C)
- U = overall heat-transfer coefficient (W/m² K)
- Ẇ = power (W)
- ΔT_{air,min} = approach temperature between ambient air and s-CO₂ (°C)
- ΔT_{HTF,min} = approach temperature between the heat-transfer fluid and s-CO₂ (°C)
- η_{comp} = compressor efficiency
- η_{exp} = expander efficiency

References

- [1] Ho, C. K., Conboy, T., Ortega, J., Afrin, S., Gray, A., Christian, J. M., Bandyopadhyay, S., Kedare, S. B., Singh, S., and Wani, P., 2014, “High-Temperature Receiver Designs for Supercritical CO₂ Closed-Loop Brayton Cycles,” *ASME Paper No. ES2014-6328*.
- [2] Iverson, B. D., Conboy, T. M., Pasch, J. J., and Kruijenga, A. M., 2013, “Supercritical CO₂ Brayton Cycles for Solar-Thermal Energy,” *Appl. Energy*, **111**, pp. 957–970.
- [3] Turchi, C. S., Ma, Z. W., Neises, T. W., and Wagner, M. J., 2013, “Thermodynamic Study of Advanced Supercritical Carbon Dioxide Power Cycles for Concentrating Solar Power Systems,” *ASME J. Sol. Energy Eng.*, **135**(4), p. 041007.
- [4] Neises, T., and Turchi, C., 2014, “A Comparison of Supercritical Carbon Dioxide Power Cycle Configurations With an Emphasis on CSP Applications,” *Solarpaces 2013 International Conference*, Vol. 49, pp. 1187–1196.
- [5] Wright, S. A., Pickard, P. S., Fuller, R., Radcl, R. F., and Vernon, M. E., 2009, “Supercritical CO₂ Brayton Cycle Power Generation Development Program and Initial Test Results,” *ASME Paper No. POWER2009-81081*.
- [6] Fruttschi, H. U., 2005, *Closed-Cycle Gas Turbines: Operating Experience and Future Potential*, ASME Press, New York, p. 283.
- [7] U.S. DOE Nuclear Energy Research Advisory Committee and Generation IV International Forum, 2002, “A Technology Roadmap for Generation IV Nuclear Energy Systems,” U.S. DOE Nuclear Energy Research Advisory Committee and the Generation IV International Forum, Washington, DC, No. GIF-002-00.
- [8] Feher, E. G., 1968, “The Supercritical Thermodynamic Power Cycle,” *Energy Convers.*, **8**(2), pp. 85–90.
- [9] Kacludis, A., Lyons, S., Nadav, D., and Zdankiewicz, E., 2012, “Waste Heat to Power (WH2P) Applications Using a Supercritical CO₂-Based Power Cycle,” *Power—Gen International 2012*, Orlando, FL, Dec. 11–13, pp. 11–13.
- [10] Persichilli, M., Held, T., Hostler, S., and Zdankiewicz, E., 2011, “Transforming Waste Heat to Power Through Development of a CO₂-Based Power Cycle,” *Electric Power Expo 2011*, Rosemount, IL, pp. 10–12.
- [11] Persichilli, M., Kacludis, A., Zdankiewicz, E., and Held, T., 2012, “Supercritical CO₂ Power Cycle Developments and Commercialization: Why s-CO₂ Can Displace Steam,” *Power-Gen India & Central Asia 2012*, Pragati Maidan, New Delhi, India, Apr. 19–21.
- [12] Held, T. J., Hostler, S., Miller, J. D., Vermeersch, M., and Xie, T., 2013, “Heat Engine and Heat to Electricity Systems and Methods With Working Fluid Mass Management Control,” *U.S. Patent No. US8613195B224*.
- [13] Angelino, G., 1968, “Carbon Dioxide Condensation Cycles for Power Production,” *ASME J. Eng. Power*, **90**(3), pp. 287–295.
- [14] Dyreby, J., Klein, S., Nellis, G., and Reindl, D., 2014, “Design Considerations for Supercritical Carbon Dioxide Brayton Cycles With Recompression,” *ASME J. Eng. Gas Turbines Power*, **136**(10), p. 101701.
- [15] Gavic, D. J., 2012, “Investigation of Water, Air, and Hybrid Cooling for Supercritical Carbon Dioxide Brayton Cycles,” Masters thesis, University of Wisconsin-Madison, Madison, WI.
- [16] Hoffmann, J. R., and Feher, E. G., 1971, “150 Kwe Supercritical Closed Cycle System,” *ASME J. Eng. Power*, **93**(1), pp. 70–80.
- [17] Angelino, G., 1967, “Perspectives for Liquid Phase Compression Gas Turbine,” *ASME J. Eng. Power*, **89**(2), pp. 229–236.
- [18] Angelino, G., 1967, “Liquid-Phase Compression Gas Turbine for Space Power Applications,” *J. Spacecr. Rockets*, **4**(2), pp. 188–194.
- [19] Angelino, G., 1969, “Real Gas Effects in Carbon Dioxide Cycles,” *ASME Paper No. 69-GT-102*.

- [20] Angelino, G., 1971, "Real Gas Effects in Carbon Dioxide Cycles," *Atomkernenergie*, **17**(1), pp. 27–33.
- [21] Angelino, G., 1978, "Use of Liquid Natural-Gas as Heat Sink for Power Cycles," *ASME J. Eng. Power*, **100**(1), pp. 169–177.
- [22] Dostal, V., Hejzlar, P., and Driscoll, M. J., 2006, "High-Performance Supercritical Carbon Dioxide Cycle for Next-Generation Nuclear Reactors," *Nucl. Technol.*, **154**(3), pp. 265–282.
- [23] Kimzey, G., 2012, "Development of a Brayton Bottoming Cycle Using Supercritical Carbon Dioxide as the Working Fluid," Electric Power Research Institute, *University Turbine Systems Research Program*, Gas Turbine Industrial Fellowship, Palo Alto, CA.
- [24] Garg, P., Sriram, H. K., Kumar, P., Conboy, T., and Ho, C., 2014, "Advanced Low Pressure Cycle for Concentrated Solar Power Generation," *ASME Paper No. ES2014-6545*.
- [25] Driscoll, M. J., and Hejzlar, P., 2004, "300 MWe Supercritical CO₂ Plant Layout and Design," Center for Advanced Nuclear Energy Systems, MIT Nuclear Engineering Department, Cambridge, MA, *Topical Report No. MIT-GFR-014*.
- [26] Schlenker, H. V., 1974, "Cost Functions for HTR-Direct-Cycle Components," *Atomkernenergie*, **22**(4), pp. 226–235.
- [27] ESDU, 1994, "Selection and Costing of Heat Exchangers," Engineering Sciences Data Unit, London, UK, No. ESDU 92013.
- [28] Peters, M. S., Timmerhaus, K. D., and West, R. E., 2003, *Plant Design and Economics for Chemical Engineers*, 5th ed., McGraw-Hill, New York, p. 988.
- [29] Siegel, N. P., Ho, C. K., Khalsa, S. S., and Kolb, G. J., 2010, "Development and Evaluation of a Prototype Solid Particle Receiver: On-Sun Testing and Model Validation," *ASME J. Sol. Energy Eng.*, **132**(2), p. 021008.
- [30] Kolb, G. J., Ho, C. K., Mancini, T. R., and Gary, J. A., 2011, "Power Tower Technology Roadmap and Cost Reduction Plan," Sandia National Laboratories, Albuquerque, NM, *Report No. SAND2011-2419*.
- [31] Falcone, P. K., Noring, J. E., and Hruby, J. M., 1985, "Assessment of a Solid Particle Receiver for a High Temperature Solar Central Receiver System," Sandia National Laboratories, Livermore, CA, *Report No. SAND85-8208*.